minerals

Article

Geochemistry, Detrital Zircon U-Pb Geochronology, and Lu-Hf Isotopes of the Metasedimentary Rocks (Xinghongpu Formation, Late Devonian) in the Central South Qinling Orogenic Belt: Implications for Provenance and Tectonics

Zhenkai Zhang [1,2], Tengfei Zhou [1,3,*], Dongtao Li [4], Hua Wang [4], Biao Du [1], Duanchang Zhao [1], Yafeng Zhang [1], Chen Zhang [1], Zuochen Li [5], Ning Chen [1], Xinlei Zhang [1] and Yuehan Shang [3]

1 Shaanxi Satellite Application Center for Natural Resources, Shaanxi Institute of Geological Survey, Xi'an 710119, China
2 Research Center of Intelligent Geological Survey, Northwestern Polytechnical University, Xi'an 710072, China
3 School of Geosciences, China University of Petroleum (East China), Qingdao 266580, China
4 Institute of Geology of the Fifth Oil Production Plant, PetroChina Changqing Oilfield Company, Xi'an 710000, China
5 School of Earth Science and Resources, Chang'an University, Xi'an 710054, China
* Correspondence: zhoutfgeoscience@126.com

Abstract: The Xinghongpu Formation is very important for understanding the Devonian tectonic evolution of the South Qinling orogenic belt. Geochemical, detrital zircon U-Pb-Hf isotopic studies were carried out on the Late Devonian metasedimentary rocks of the Xinghongpu Formation to constrain the depositional age, the provenance, and the tectonic setting. The detrital zircon U-Pb dating results revealed that the depositional age of the Xinghongpu Formation of the Late Devonian was not earlier than 363.2 Ma. The whole-rock geochemistry suggested that (1) this suite of metasedimentary rocks was mainly derived from quartzose sediments of mature continental provenance, with a small contribution from mafic and intermediate igneous provenance, and (2) the metasedimentary sandstone of the Xinghongpu Formation from the Late Devonian was deposited in an active continental margin to continental arc setting. The detailed detrital zircon U-Pb dating showed that the age spectra of detrital zircon could be divided into four groups: (1) 416–480 Ma, accounting for about 23%; (2) 740–850 Ma, accounting for about 19%; (3) 889–1017 Ma, accounting for about 19%; and (4) 1072–1146 Ma, accounting for about 12%. It also contained a group of Early Proterozoic zircons. The age and Hf isotope of the detrital zircons suggested that the clastic sediment deposited in the Xinghongpu Formation mainly came from the South Qinling Orogenic Belt and the North Qinling Orogenic Belt. The detrital zircon Lu-Hf isotopes indicated that most zircons were the products of the ancient crustal remelting, and the mantle-derived magmatic sources contributed to the provenance. The Xinghongpu Fm. formed in an oceanic basin in a continental margin environment with arc systems.

Keywords: detrital zircon; U-Pb dating and Lu-Hf isotope; late Devonian; South Qinling orogenic belt

Citation: Zhang, Z.; Zhou, T.; Li, D.; Wang, H.; Du, B.; Zhao, D.; Zhang, Y.; Zhang, C.; Li, Z.; Chen, N.; et al. Geochemistry, Detrital Zircon U-Pb Geochronology, and Lu-Hf Isotopes of the Metasedimentary Rocks (Xinghongpu Formation, Late Devonian) in the Central South Qinling Orogenic Belt: Implications for Provenance and Tectonics. *Minerals* **2023**, *13*, 768. https://doi.org/10.3390/min13060768

Academic Editors: Kaijun Zhang and Xianchun Tang

Received: 24 February 2023
Revised: 22 May 2023
Accepted: 26 May 2023
Published: 2 June 2023

1. Introduction

The Qinling orogenic belt (QOB) in central China is a very important part of the Central Orogenic Belt [1,2]. It is between the North China Craton (NCC) in the north and the South China Craton (SCC) in the south. The west of the QOB is connected with the Qilian-Kunlun-Algin orogenic belt and the Pamir Plateau, and the southwest is adjacent to the Songpan-Ganzi fold belt. The east of the QOB is connected with the Tongbai-Hong'an-Dabie-Sulu orogenic belt [3–5]. The QOB has been divided into several parts [1]: the southern margin of the NCC (S-NCC), the North Qinling belt (NQB), and the South Qinling belt (SQB). These three terranes are separated from each other by the Shangdan Suture

Zone (SSZ) in the north and the Mianlue Suture Zone (MSZ) in the south [1,6]. Like the other major collisional orogenic belts in the world, the QOB was also constructed through prolonged processes of arc–arc, arc–continent, and continent–continent collisional events [7–9]. Its main collisional tectonic period was from the late Archaean to the Middle Triassic. The QOB experienced a long and complex collisional process from the rifting system to a plate collisional system, varying from extensional to subducting and then to a collisional environment [10–12]. The tectonic evolution was recorded and can be reflected by the sedimentary layers in the QOB, which was divided into five main parts from the old to the present: (1) the basement rock, which is Archean–Paleoproterozoic metamorphic rocks; (2) Neoproterozoic metasedimentary rocks and igneous rocks; (3) Mesoproterozoic–Paleozoic ophiolitic suites; (4) Paleozoic metasedimentary rocks, migmatites, and HP-UHP metamorphic rocks; and (5) Paleozoic–Mesozoic granitoid plutons [1,6,13]. To constrain the tectonic evolution of the QOB more clearly, a large amount of research has been carried out on the geochemical and geochronological features of the different layers in the QOB. Dong et al. [13] studied the Kuanping ophiolite, which represents a Mesoproterozoic ocean, which helps ensure the time of the amalgamation of the north Qinling Terrain to the North China Craton. The geochemical and geochronological study on the adakitic rocks and the complex in the NQB reflect the subduction of the Qinling oceans and the tectonic setting [14–16]. Furthermore, the pre- and post-collisional processes were also uncovered by the geochemical and geochronological study on granite in the QOB [17,18].

In addition, in recent years, the detrital zircon U-Pb dating and Hf isotope were widely applied in the analysis of tectonic evolution and provenance in basin and orogeny research [19–23]. In addition, some research was carried out with the help of detrital zircon dating in the QOB. Yang et al. [24] analyzed the provenance of the Jiyuan basin with detrital zircon U-Pb data and established the unroofing pattern of the QOB. Zhang et al. [25] investigated the Late Paleozoic and Early Mesozoic tectonic and paleogeographic evolution of central China through the study of the detrital zircon from the western QOB. The tectonic evolution and sedimentary provenance of the basin in the NQB, such as the Liuyehe basin and Lingguanmiao basin, were analyzed with the detrital zircon dating result of metamorphic sedimentary rocks, showing the slab–arc–basin system in the NQB from the Late Paleozoic to the Early Mesozoic [26,27] and the new intracontinental orogeny after the Indosinian orogeny [28]. In addition, the whole-rock geochemistry of metasedimentary rocks was used to study the sedimentary provenance in the QOB [29]. Dai et al. [30] studied the geochemical characteristics of meta-mud-siltstones from the Danfeng ophiolite mélange and found they were formed during the Ordovician to the Silurian, and the sedimentary set should be in a fore-arc basin of the active continental margin. When compared with the NQB, the geological story of the SQB has not been fully uncovered. Especially in our study area, Fengxian town, most of the detrital zircon studies of sedimentary rocks are focused on the Early to Middle Devonian [31–34], while there are fewer reports about the layers of the Late Devonian. This study focused on the Late Devonian Xinghongpu Formation (Fm.) in the Fengxian area, using whole-rock geochemistry, detrital zircon U-Pb dating, and Lu-Hf isotopes to uncover the sedimentary provenance and tectonic setting for the metasedimentary rocks from the Xinghongpu Fm. It was a supplementary study to the research on the sedimentary provenance and tectonic evolution of the SOB.

2. Geological Setting

The SQB has experienced a complex tectonic evolution. From the end of the Neoproterozoic to the beginning of the early Paleozoic, the ancient Qinling Ocean opened and gradually created an intensive extensional environment. This extensional environment lasted until the Middle Ordovician and then transferred to the convergence stage with the Yangtze plate subducting to the North China Craton. Thus, the SQB became the passive continental margin of the Yangtze plate [10]. At the same time, the northern margin of the Yangtze plate entered into a new extensive environment in the early Devonian. During this process, the Mianlue Ocean formed [11,23], which caused the separation of the passive continental margin of the SQB from the Yangtze plate [3]. During the same period, a rifting zone developed along Minxian-Lixian-Fengzheng-Shanyang, forming a series of marine basins such as Zhengxun, Zhashan, Bansha, Fengtai, Xicheng, and Limin [35]. The Fengxian area is located in the central SQB (Figure 1). The exposed layers in the Fengxian are mainly Devonian, including the Middle Devonian Dafenggou Fm., the Middle–Late Devonian Gudaoling Fm., and the Late Devonian Xinghongpu Fm. and Jiuliping Fm. [36]. The Gudaoling Fm. and the Xinghongpu Fm. have promising potential for the exploration of lead-zinc and gold deposits. In addition, the Cretaceous Donghe group is also widely spread in the study area, which is the deposits of the Mesozoic rift basin [37,38].

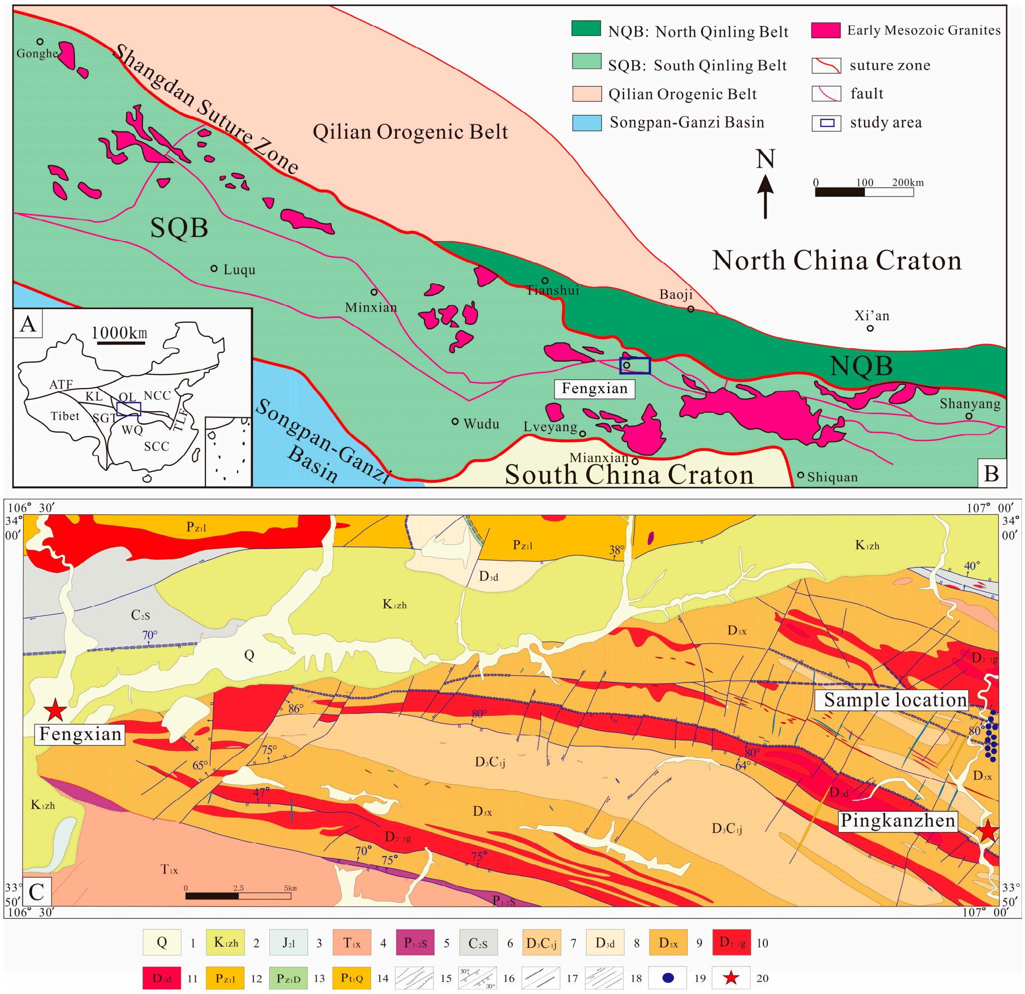

Figure 1. Geological maps of the study area (modified from [36]). (**A**) Geotectonic sketch map of China. (**B**) Tectonic framework map of the Qinglin Orogenic Belt. (**C**) Geological map of the Fengxian district showing sampling location. Legend: 1—Quaternary; 2—the Lower Cretaceous Zhoujiawan Fm.; 3—the Middle Jurassic Longjiawan Fm.; 4—the Lower Triassic Xipo Fm.; 5—the Lower–Middle Permian Shuixiakou Fm.; 6—the Upper Carboniferous Sixiakou Fm.; 7—the Upper Devonian Jiuliping Fm.; 8—the Upper Devonian Dacaotan Fm.; 9—the Upper Devonian Xinghongpu Fm.; 10—the Middle–Upper Devonian Gudaoling Fm.; 11—the Middle Devonian Dafenggou Fm.; 12—the Lower Paleozoic Luohanzi Fm.; 13—the Lower Paleozoic Danfeng Group; 14—the Lower Proterozoic Qinling Group; 15—geological boundary; 16—small fault; 17—brittle-ductile shear zone; 18—regional fault; 19—sampling location; 20—town.

The Xinghongpu Fm. is characterized by a huge suite of muddy sediments, which can be divided into three parts from the bottom to the top [35]. Part 1 generally consists of slightly metamorphic clastic rocks intercalated with carbonate rocks. This part changed upward with less calcium and more siliceous clastic. Part 2 mainly consists of muddy components, with light green silty metasedimentary rock at the bottom. Calcium deposits appeared as interlayers, such as silty limestone, in the middle and upper parts of this part. The content of calcium in part 2 is higher than in part 1. Part 3 shows a similar lithological variation to part 2. The lower part of part 3 is fine clastic rocks and mudstone without any calcium deposits, while the calcium deposits developed as interlayers in the middle part of part 3. The upper part of part 3 is characterized by thin muddy carbonate rock. The overlying layer of part 3 from the Xinghongpu Fm. belongs to the Jiuliping Fm., which spans the Late Devonian and the Early Carboniferous. It is marked with many more carbonate deposits than what was developed in the Xinghongpu Fm. The metamorphic degree of the sedimentary rocks from the Jiuliping Fm. is also higher than the one developed in the Xinghongpu Fm. Thus, the sedimentary rocks from the Xinghongpu Fm. are more suitable to understand the sedimentary provenance and tectonic setting of the QOB in the Late Devonian. In this study, we picked 12 samples of slightly metamorphic siltstone of the Xinghongpu Fm. along the profile that is 50 km east of Fengxian County and 5 km north of Pingkan Town (Figure 1C). The metamorphic sandstone is yellow or green as a weathered color in the field (Figure 2A) and demonstrates a microscopically blastopsammitic texture (Figure 2B).

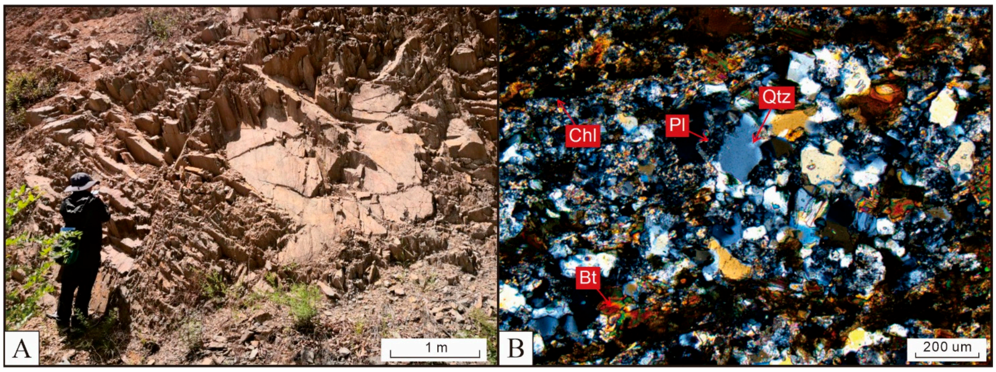

Figure 2. Field photo (**A**) and photomicrographs (**B**) of metamorphic siltstone from the Xinghongpu Fm. Qtz—quartz; Pl—plagioclase; Bt—biotite; Chl—chlorite.

3. Methods

3.1. Whole-Rock Elemental Geochemistry

The chemical analyses were conducted at the geochemistry lab of Geomillion Mineral Testing Technology Co., Ltd., Xi'an, China. Before the experiment, fresh rock pieces without cracks were crushed to a 200 mesh size. The major oxides were analyzed by X-ray fluorescence spectrometry (XRF; equipment model is Axios) with the relative standard derivation (2RSD) of major oxides less than 5%. The procedure for the major element analyses was described by Kimura [39]. The trace elements were analyzed by ICP-MS (equipment model was ICAP Qc), and the detailed procedures for the trace element analysis were described by Liang et al. [40]. The relative standard deviations (RSDs) of trace elements were within 5%.

3.2. LA-ICP-MS Zircon U-Pb Dating

The U-Pb dating and trace element analyses of zircon were conducted synchronously by LA-ICP-MS at the geochemistry lab of Geomillion Mineral Testing Technology Co., Ltd. The laser sampling was performed using a New wave NWR213. An Agilent 7500ce ICP-MS instrument was used to acquire ion signal intensities. Helium was applied as a carrier gas. Argon was used as the make-up gas and mixed with the carrier gas via a T connector before entering the ICP. Each analysis incorporated a background acquisition of approximately 10 s (gas blank) followed by 40 s data acquisition from the sample. The

Agilent Chemstation was utilized for the acquisition of each analysis. Off-line selection and integration of background and analyte signals, time drift correction, and quantitative calibration for trace element analyses and U-Pb dating were performed by Glitter 4.4. Zircon 91,500 was used as an external standard for U-Pb dating. Time-dependent drifts of U-Th-Pb isotopic ratios were corrected using linear interpolation (with time). The preferred U-Th-Pb isotopic ratios used for 91,500 were from Wiedenbeck et al. [41]. The uncertainty of the preferred values for the external standard 91,500 was propagated to the ultimate results of the samples. Concordia diagrams were created and weighted mean calculations were performed using Isoplot/Ex_ver3 [42]. The trace element compositions of zircons were calibrated against reference materials (NIST610) combined with Si as an internal standardization. The preferred values of the element concentrations for the NIST reference glasses were from the GeoReM database, http://georem.mpch-mainz.gwdg.de/sample_query_pref.asp (accessed on 25 May 2023). In addition, the age concordance of the zircons was not less than 80%, while the lower ones were eliminated. The zircon U-Pb dating method was described in detail by Duan [43].

3.3. Zircon In Situ Lu-Hf Isotope

The in situ zircon Hf isotope analyses were performed using a New Wave UP213 laser ablation microprobe coupled to a Neptune MC–ICP–MS at the geochemistry lab of Geomillion Mineral Testing Technology Co., Ltd. Meng et al. [44] described the method of testing in situ Lu-Hf isotopes in detail. A stationary spot with a beam diameter of 40 or 55 um was used. Helium was used as a carrier gas and was combined with argon in a mixing chamber before being introduced to the ICP–MS plasma. The values of $^{176}Lu/^{175}Lu$ = 0.02658 and $^{176}Yb/^{173}Yb$ = 0.796218 were used to correct for the ^{176}Lu and ^{176}Yb isobaric interferences, respectively [45]. The zircon GJ1 was used as the reference standard, yielding a weighted mean $^{176}Hf/^{177}Hf$ value of 0.282008 $\pm$ 27 (2σ). All Hf isotope data were reported with an error of 2σ of the mean, and values of ε_{Hf} were calculated using a ^{176}Lu decay constant of 1.865×10^{-11} yr^{-1} [46]. The depleted mantle model ages (TDMs) were calculated based on the measured $^{176}Lu/^{177}Hf$ and $^{176}Hf/^{177}Hf$ values concerning the depleted mantle with present-day $^{176}Hf/^{177}Hf$ = 0.28325 and $^{176}Lu/^{177}Hf$ = 0.0384 [47]. The average continent crustal (TC DM) model ages were calculated for the magma source using the zircon's initial $^{176}Hf/^{177}Hf$ value, assuming a mean crustal value of 0.015 [48].

4. Results

The major element, trace element, and rare earth element contents of 12 samples analyzed in this study are listed in Supplementary Table S2. The zircon U-Pb dating and Lu-Hf isotopic results of the sample PM02-2 are presented in Supplementary Table S1.

4.1. Major Elements

The element composition of the metasedimentary rocks was dominated by SiO_2 (48.7~69.4 wt.%, average 61.1 wt.%), Al_2O_3 (7.55~18.1 wt.%, average 14.2 wt.%), and CaO (1.48~14.9 wt.%, average 5.85 wt.%). In addition, these rocks also contained relative low concentrations of Fe_2O_3 (3.05~7.37 wt.%, average 6.00 wt.%), K_2O (0.54~4.28 wt.%, average 2.56 wt.%), MgO (1.51~5.93 wt.%, average 3.31 wt.%), and Na_2O (0.85~4.46 wt.%, average 1.99 wt.%). The contents of other major elements (MnO, P_2O_5, and TiO_2) were all lower than 1 wt.%. The average contents of SiO_2, Al_2O_3, Fe_2O_3, K_2O, TiO_2, P_2O_5, and MnO of our samples were close to PAAS, while the content of CaO was much higher than the one in PASS (Figure 3). The contents of MgO and Na_2O were a bit higher than the ones in PASS.

There was a negative correlation between the contents of SiO_2 and Al_2O_3 and between the contents of Al_2O_3 and CaO (Figure 4). No obvious correlation could be observed between the contents of Al_2O_3 and P_2O_5. However, the samples showed a positive correlation between the contents of Al_2O_3 and TiO_2, between the contents of Al_2O_3 and TFe_2O_3, and between the contents of Al_2O_3 and K_2O. The rocks were compositionally variable, but most samples shared similar geochemical characteristics (Figure 5), as shown by their respective lg(SiO_2/Al_2O_3) (0.52~0.94) and lg(TFe_2O_3/K_2O) (0.17~1.07) values. Most samples fell within the shale and wacke fields on Herron's sedimentary rock classification diagram [49] (Figure 5), while three samples fell in the Fe-Shale, Fe-sand, and Lith-arenite fields.

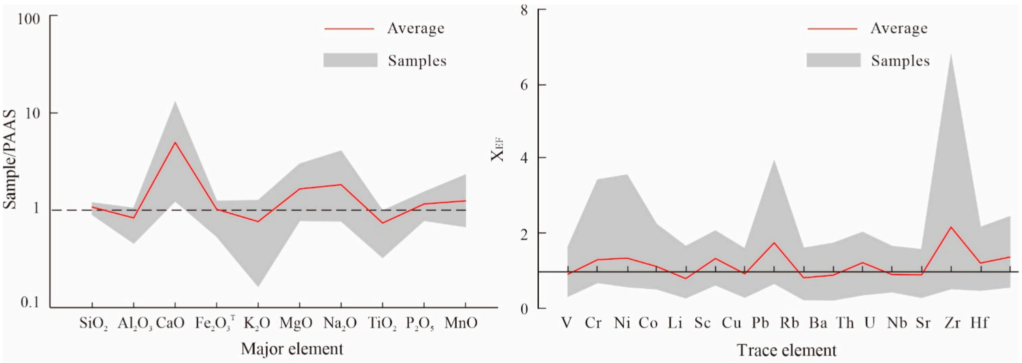

Figure 3. Major elements normalized by PAAS and XEF of trace elements of metasediment rocks from the Xinghongpu Fm.

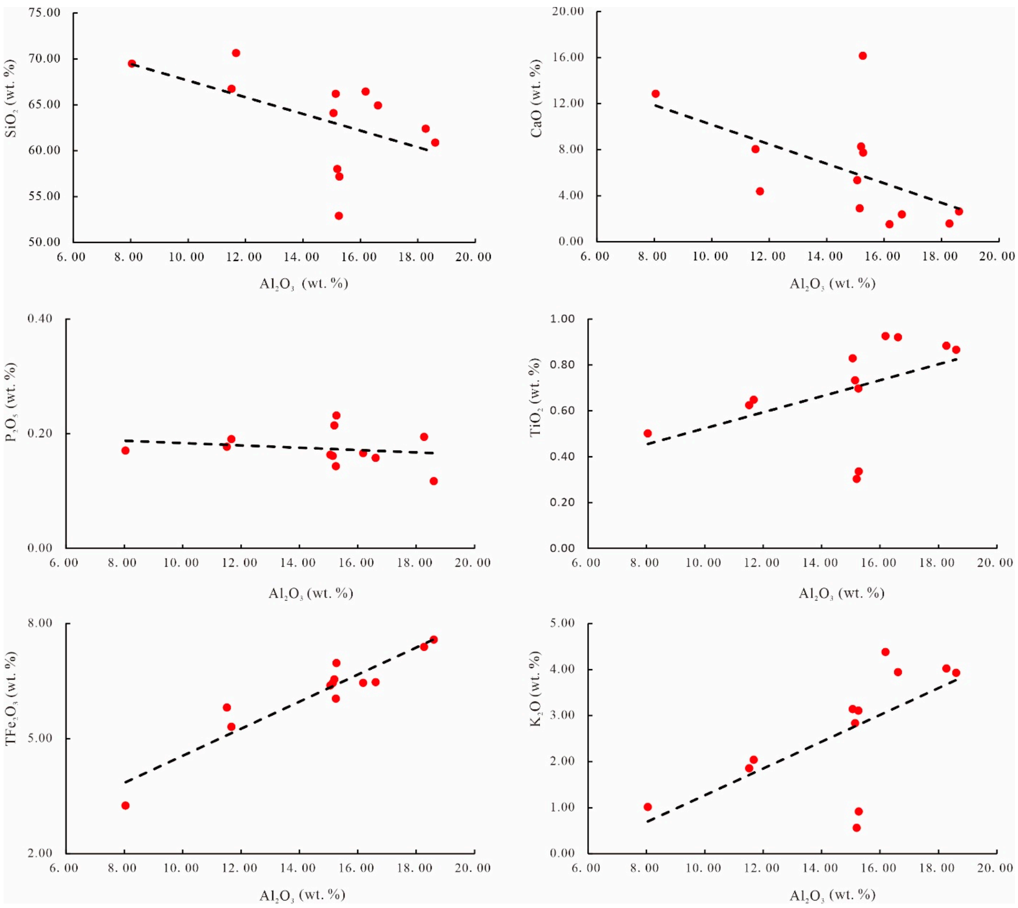

Figure 4. The Harker diagrams of major elements of metasedimentary rocks from the Xinghongpu Fm.

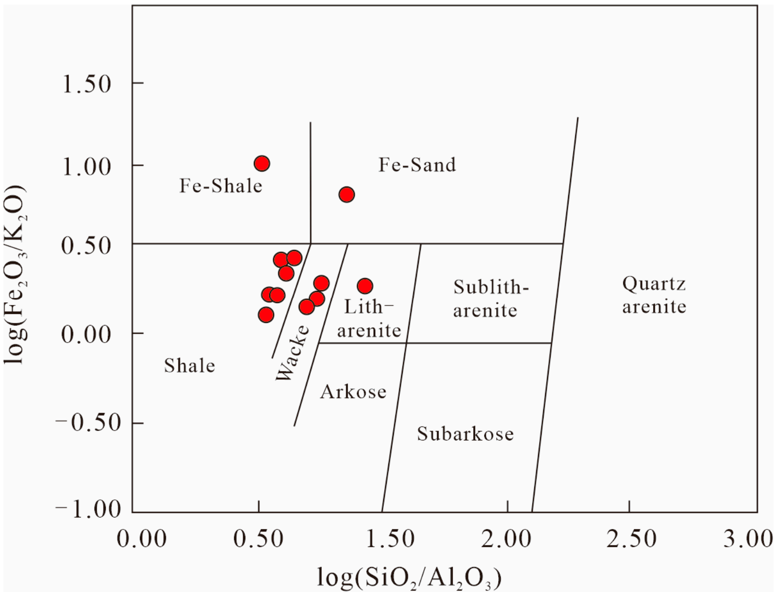

Figure 5. Log(Fe_2O_3/K_2O) vs. log(SiO_2/Al_2O_3) diagram (modified after [49]) for metasedimentary rocks from the Xinghongpu Fm.

4.2. Trace and Rare Earth Elements

Element enrichment factors were used to see the enrichment or depletion of an element by comparing it with a selected standard value. In this study, the trace elemental compositions of the samples were compared with the composition of PAAS [50] through Al-normalization to identify significant deviations [51]. Element enrichment factors of X (X_{EF}) were calculated by $X_{EF} = (X/Al)_{Sample}/(X/Al)_{PAAS}$. $X_{EF} > 1$ represents that element X was relatively enriched in the sample compared with X in PAAS, while $X_{EF} < 1$ represents the situation of depletion [51]. The X_{EF} values of Cr, Co, Ni, Sc, Pb, Th, Sr, Zr, and Hf were larger than 1, showing these trace elements were more enriched in the samples than in PAAS, while the X_{EF} values of Li and Rb were much lower than 1, indicating these elements were depleted. As to the elements V, Cu, Ba, U, and Nb, the X_{EF} values were close to 1, indicating that they behaved similarly to PAAS. The total ∑REE content of the Xinghongpu Fm. metasedimentary rocks varied from 106 ppm to 204 ppm. Moreover, the samples were enriched in LREE (96.1~182 ppm) relative to HREE (10.1~22.0 ppm) and showed prominent negative Eu anomalies (δEu = 0.58~0.89), and the ratio of $(La/Yb)_N$ was 7.89~11.8 (Supplementary Table S2).

4.3. Detrital Zircon U-Pb Dating

The analytical data are presented in Supplementary Table S1. Eighty zircons of the sample PM01 were selected for U-Pb analysis, and 75 spots produced good results. The zircons could be easily divided into two groups based on their CL image (Figure 6). Most zircons contained oscillatory growth zoning and yielded relatively high Th/U values (0.20~2.45), indicating a magmatic origin [44,52,53]. They are typically subhedral to euhedral, subrounded to subangular, and 35~100 μm in size. Two of these zircons were internally homogeneous with low Th/U values (less than 0.1) and were rounded and allotriomorphic in shape, suggesting a metamorphic origin [54–56]. The youngest zircon yielded an age of 363.2 ± 3.2 Ma with a magmatic zircon Th/U ratio (0.84), and the oldest zircon yielded an age of 2502 ± 13 Ma (Figure 7A). The main age peaks of these zircons were at about 440 Ma, 826 Ma, 970 Ma, and 1100 Ma (Figure 7B). They also contained a lot of old zircons, whose ages ranged from 1200 to 2500 Ma.

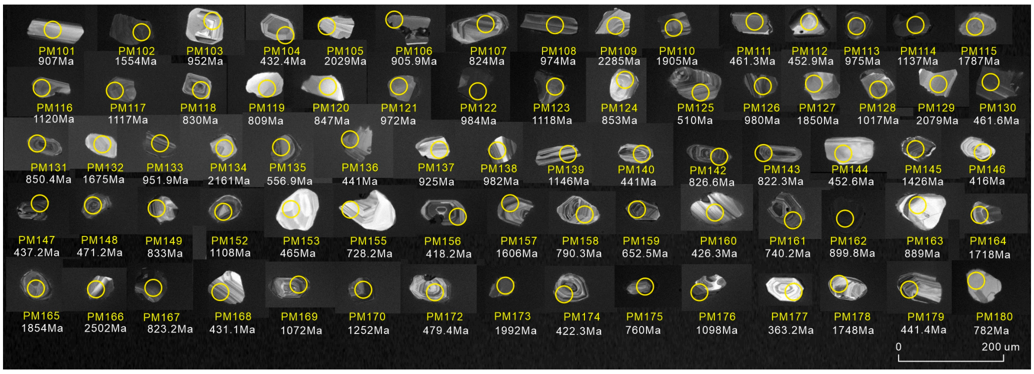

Figure 6. CL image of zircons of PM01 from the Xinghongpu Fm. The CL images of zircons 141, 150, 151, and 171 are not presented because their age concordance was lower than 80%, and zircon 154 was eliminated for its bad result during the test.

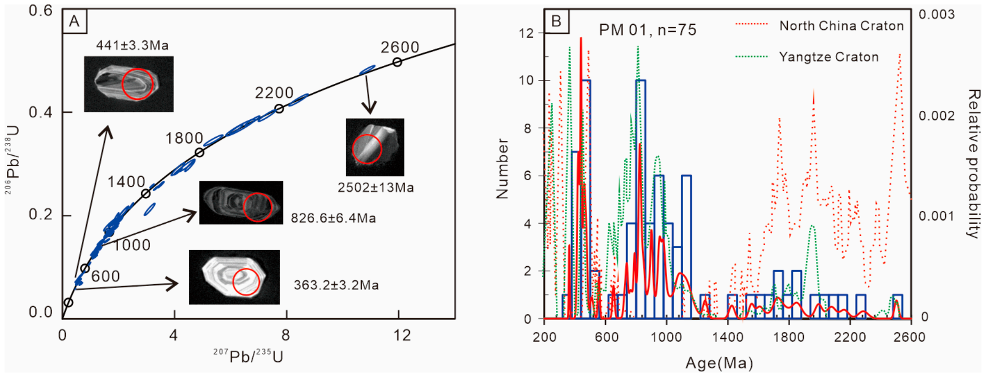

Figure 7. Zircon U-Pb concordia diagram (**A**) and frequency histograms (**B**) of PM01 from the Xinghongpu Fm. The probability densities of the Yangtze craton and the North China craton are from [34].

4.4. Zircon Lu-Hf Isotope

Zircon in situ Lu-Hf isotopic compositions of the dated 75 grains were also measured (Supplementary Table S1). The values of ^{176}Hf/^{177}Hf of these analytical spots ranged from 0.281234 to 0.283003, and the values of ^{176}Lu/^{177}Hf of these analytical spots ranged from 9.5×10^{-5} to 6.858×10^{-3}. The corresponding values of ε_{Hf}(t) had a wide range interval from −22.58 to +16.26, with most grains (>70%) giving negative ε_{Hf}(t). The ε_{Hf}(t) value showed different characteristics in different age ranges. The number of zircons with positive ε_{Hf}(t) values nearly equaled the ones with negative ε_{Hf}(t) values when their ages were older than 1000 Ma, while the zircons with negative ε_{Hf}(t) values dominated when their ages were younger than 1000 Ma. The model ages (T_{DM2}) were from 401 to 3141 Ma. Almost all the zircons demonstrated that their model ages (T_{DM2}) were larger than their ^{206}Pb/^{238}U or ^{207}Pb/^{206}Pb ages, while one zircon with 461 Ma as its ^{206}Pb/^{238}U age showed the opposite.

5. Discussion

5.1. Depositional Age of the Xinghongpu Fm

Detrital zircon's age was usually used to ensure the earliest depositional age of the layers because the deposition could not happen before the formation of the zircon, which came from its provenance. As shown above, the youngest age found when dating the zircon analyzed in this study was 363.2 ± 3.2 Ma (Figure 7A), indicating that the depositional age of the Xinghongpu Group should be younger than 363.2 Ma. In addition, the biological assemblage of the Xinghongpu Formation was classified into the Ancyrodella rotundiloba alata assemblage zone, which belonged to the Late Devonian.

Combined with the regional geological setting, this implied that the Xinghongpu group should belong to the latest Devonian.

5.2. Provenance

5.2.1. Evidence from Whole-Rock Geochemistry

The sedimentary geochemistry of rocks, detrital zircon geochronology, and zircon Lu-Hf isotope are useful tools widely used to distinguish the provenance of sediments.

Roser and Korsch [57] defined two functions (F1 and F2) to help distinguish the sediments from different provenances, including P1 (primarily mafic and lesser intermediate igneous provenance), P2 (primarily intermediate igneous provenance), P3 (felsic igneous provenance), and P4 (quartzose sediments of mature continental provenance):

$$F1 = -1.773 \times TiO_2 + 0.607 \times Al_2O_3 + 0.76 \times TFe_2O_3 - 1.5 \times MgO + 0.616 \times CaO + 0.509 \times Na_2O - 1.224 \times K_2O - 9.09,$$

$$F2 = 0.445 \times TiO_2 + 0.07 \times Al_2O_3 - 0.25 \times TFe_2O_3 - 1.142 \times MgO + 0.438 \times CaO + 1.475 \times Na_2O + 1.426 \times K_2O - 6.861.$$

Most of our samples fell into the P4 zone, while two fell into the P1 zone, and the others fell into the P2 zone (Figure 8). It suggests that quartzose sediments of mature continental provenance were the main provenance of the Xinghongpu Fm., and the mafic and intermediate igneous provenance also contributed to the Xinghongpu Fm. Floyd and Leveridge [58] proposed the Hf vs. La/Th diagram to distinguish the sedimentary source. Our sample fell into the field of acidic arc source with a mixed felsic and basic source and some ancient crustal material (Figure 9). In the Th/Sc-Zr/Sc diagram (Figure 10), two of our samples show different chemical compositions from the other samples. These two samples should be closely related to a mafic to intermediate igneous source marked by high Fe content (Figures 8 and 9) and very close to the andesite (Figure 10). In addition, the other samples did not show any compositional variation, suggesting they may not have originated from igneous provenance (Figure 10). It suggests they should be controlled by the mature continental source whose main compositional mineral was dominated by quartz and feldspar.

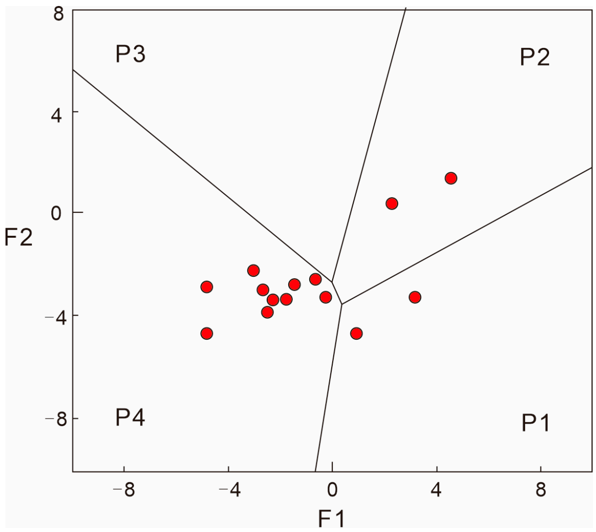

Figure 8. F1-F2 function diagram to distinguish provenance [57]. P1, primarily mafic and lesser intermediate igneous provenance; P2, primarily intermediate igneous provenance; P3, felsic igneous provenance; and P4, quartzose sediments of mature continental provenance.

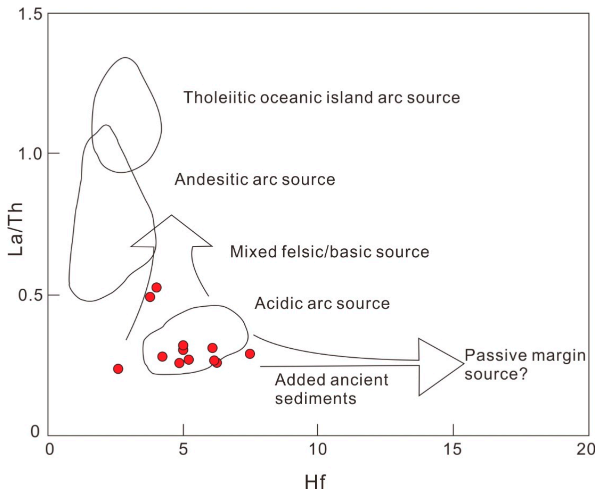

Figure 9. Sedimentary source (Hf vs. La/Th; modified after [58]).

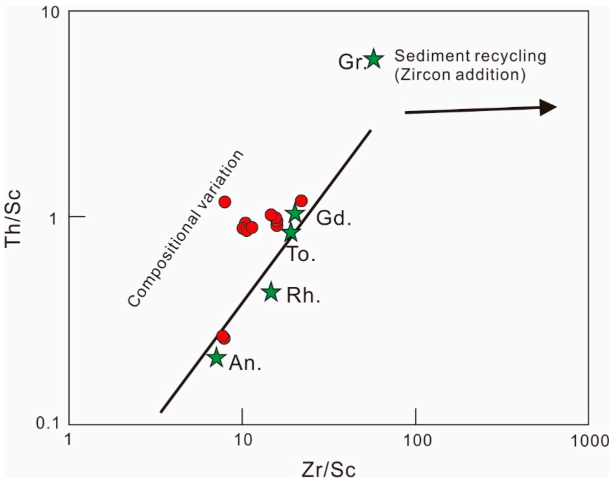

Figure 10. Th/Sc–Zr/Sc diagram after [59]. The data for tonalite (To), granodiorite (Gd), granite (Gr), and rhyolite and andesite are from [60].

5.2.2. Evidence from Detrital Zircon U-Pb Age and Hf Isotope

Combining the U-Pb age with the in situ Hf isotope of the detrital zircons could help constrain the provenance in complex situations. Seventy-five spots of detrital zircons were analyzed for their U-Pb age and the corresponding Lu-Hf isotopes. The age of the zircons ranged widely from 363.2 Ma to 2502 Ma, suggesting a complicated provenance that contained old crust material. Only two zircons from our sample were aged with a Devonian age (363.2 Ma and 416 Ma). Their ε_{Hf}(t) values were −10.83 and 0.14, respectively. The lack of zircons aged from 364 Ma to 415 Ma indicated that the paleoenvironment of the study area in Devonian was a sag or a basin that could accept the deposits from ancient sources and lacked volcanic activity. It was consistent with understanding the stratigraphy and sedimentology of the Xinghongpu Fm. The zircon frequency histogram of our sample behaved similarly to the zircon frequency histogram of the Yangtze Craton with age peaks of 440 Ma, 826 Ma, 970 Ma, and 1100 Ma, lacking in the zircon frequency histogram of the North China Craton (Figure 7B). However, the Neoproterozoic detrital zircons (~0.8 Ga) from the Yangtze Craton were marked by positive ε_{Hf}(t) values [25]. However, the ε_{Hf}(t) values of the zircons (~0.8 Ga) in our sample varied from −17.8 to 6.61 (only three of 17 showed positive values). It indicated that there were at least two sources that contributed to the provenance, suggesting a complex provenance of the Xinghongpu Fm.

The Silurian zircons of our sample were aged from 437.2 Ma to 418.2 Ma, with negative εHf(t) values (−9.9~−0.39). These were consistent with the zircons of granites and gneiss in the NQB [15,61], suggesting that the NQB should be a provenance zone of the Xinghongpu Fm. This also indicated that the igneous source provided a large amount of material as the clastics for the Xinghongpu Fm. The age of our Ordovician zircons varied from 479.4 Ma to 441 Ma. Most of them showed negative $\varepsilon_{Hf}(t)$ values (−16.75~−0.44), while the zircons aged 461.3 ~ 465 Ma showed positive $\varepsilon_{Hf}(t)$ values (2.21~16.26). The positive group was consistent with the zircons of the amphibolite in the SQB (Shi et al., 2013), while the negative one should come from the gneiss in the NQB. Only one zircon was aged with a Cambrian age of 510 Ma, showing a positive $\varepsilon_{Hf}(t)$ value (9.37). The Neoproterozoic zircons of our sample were aged from 984 Ma to 556.9 Ma, with varying $\varepsilon_{Hf}(t)$ values from −22.58 to 8.98. The latest Neoproterozoic zircons marked by positive $\varepsilon_{Hf}(t)$ values should come from the granitoid in the SQB [62], while the zircons with the age of ~820 Ma and positive $\varepsilon_{Hf}(t)$ value were very consistent with the zircons from dioritic intrusion and migmatite in Yangtze Craton [20]. The other Neoproterozoic zircons of our sample were almost marked by negative $\varepsilon_{Hf}(t)$ value, which was common in the SQB and the NQB. Most of the early Mesoproterozoic zircons (seven of 10) were marked with negative $\varepsilon_{Hf}(t)$ values (−6.42~−1.25), while the other three zircons were marked with positive $\varepsilon_{Hf}(t)$ values. It was consistent with the quartz schist in the NQB [15,63]. In addition, the middle–late Mesoproterozoic zircons of our samples were all marked with positive $\varepsilon_{Hf}(t)$ values, which was similar to the zircons of gneiss in the NQB as well [15]. The Paleoproterozoic zircons were also mostly marked by negative $\varepsilon_{Hf}(t)$ values, while the zircons (aged 1675 Ma, 1606 Ma, and 2161 Ma) were marked by positive $\varepsilon_{Hf}(t)$ values. There was only one zircon with a Neoarchean age, showing a positive $\varepsilon_{Hf}(t)$ value. These Hf isotopic characteristics of zircon are similar to the ones from the NQB [15,63].

Above all, the potential provenance of the Xinghongpu Fm. was from multiple sources, including the SQB, NQB, and Yangtze Craton. However, because the Mianlue Ocean between the SQB and Yangtze Craton opened in the Early Devonian and existed until the Middle–Late Triassic [11,23,25], it would hinder the transport of detrital material from the Yangtze Craton to the SQB in the Late Devonian. The zircons showing similar geochemical features to the Yangtze Craton were all older than 800 Ma. In that period, the SQB was an extensional oceanic zone near the Yangtze Craton and accepted the clastics from Yangtze Craton as depositions. This is why some old zircons of our sample geochemically behaved similarly to the ones in the Yangtze Craton. Thus, the provenance of the Xinghongpu Fm. was mainly the SQB and the NQB.

5.3. Crustal Evolution and Tectonics

The age and Hf isotope of detrital zircons could help understand regional tectonic evolution [23,25,64] and assess plate tectonic reconstructions [22,65] for their wide age range, which was hardly recorded by the whole rock.

5.3.1. Crustal Evolution

The age and the Hf isotopic features of zircons (Figure 11) could provide interpretations on the regional crustal evolution. The main age groups of the detrital zircons of our sample were divided into the four groups below.

Group 1 included the zircons aged from 416–480 Ma, with $\varepsilon_{Hf}(t)$ = −16.8~3.19 and T_{DM2} = 1237~2479 Ma, except for one zircon aged 461.6 Ma with $\varepsilon_{Hf}(t)$ = 16.26 and T_{DM1} = 417 Ma and, in addition, another zircon aged 510 Ma with $\varepsilon_{Hf}(t)$ = 9.37 and T_{DM1} = 750 Ma. These suggested that most of the zircons came from remelting of the ancient crust while there was a depleted-mantle-derived magmatic intrusion or volcanic deposits developing during the Ordovician and Silurian in the study area, representing the early Paleozoic crustal growth event.

Group 2 included the zircons aged from 740–1017 Ma, with $\varepsilon_{Hf}(t)$ = −22.6~8.98 and T_{DM2} = 1626~3078 Ma, except the zircons aged 823.2 Ma, 824 Ma, 982 Ma, and 1017 Ma, with positive $\varepsilon_{Hf}(t)$ values (6.53, 6.61, 8.98, and 6.5), indicating crustal growth events at ~823 Ma in the middle Neoproterozoic and at ~1000 Ma in the transitory stage from the

Mesoproterozoic to the Neoproterozoic. In addition, the other zircons were characterized by negative $\varepsilon_{Hf}(t)$ values, representing the remelting and recycling of the ancient crust.

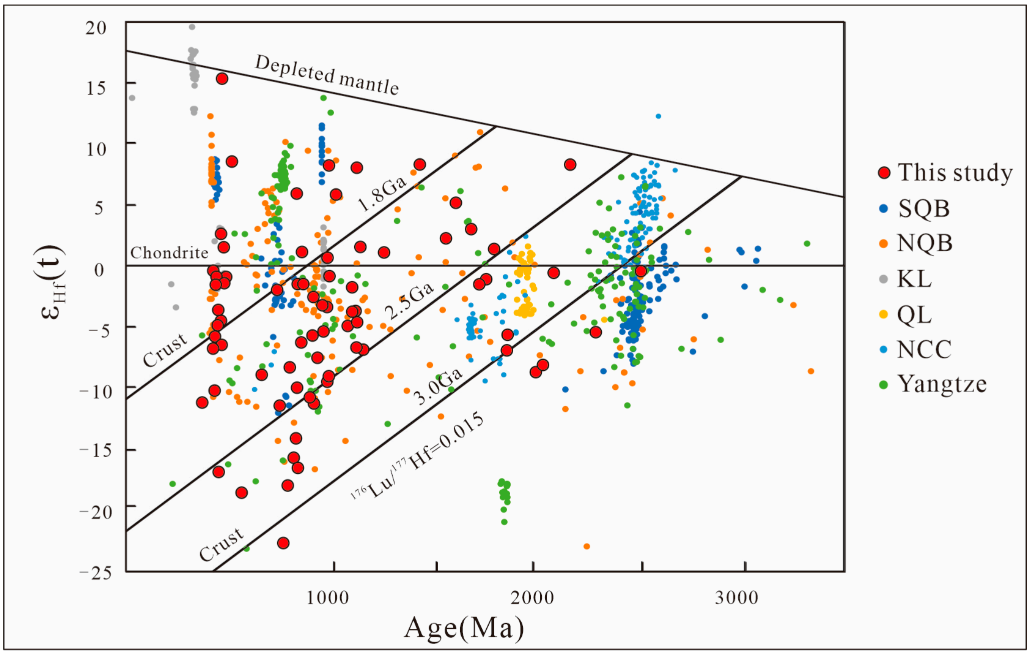

Figure 11. Age (Ma) vs. εHf(t) diagram of PM01 from the Xinghongpu Fm. Data sources: the SQB data were from [15,62,66], the NQB data were from [15,61,63], Kunlun from [67,68], the Qilian data were from [69], the North China Craton (NCC) data were from [70,71], and the Yangtze Craton (Yangtze) data were from [20,72–75].

Group 3 included the zircons aged from 1072–1787 Ma. This group of zircons could be divided into two subgroups according to the ages and different $\varepsilon_{Hf}(t)$ values: subgroup 1 (1072~1146 Ma), with $\varepsilon_{Hf}(t) = -6.42\sim-1.25$ and T_{DM2} = 1999~2361 Ma, except for two zircons aged 1120 Ma and 1137 Ma with $\varepsilon_{Hf}(t)$ = 2.14~8.81 and T_{DM1} = 1287 Ma and 1562 Ma, and subgroup 2 (1252~1675 Ma), with positive $\varepsilon_{Hf}(t) = -6.42\sim-1.25$ and T_{DM1} = 1549~1969 Ma. These indicated crustal growth events from the end of the Paleoproterozoic to the early Mesoproterozoic, while in the late Mesoproterozoic, crustal remelting took place and became dominant.

Group 4 included the zircons aged from 1718–2502 Ma, except for one zircon (age 2161 Ma), with a strong positive $\varepsilon_{Hf}(t)$ value (9.02) and T_{DM1} = 2174 Ma. The other zircons had negative or slightly positive $\varepsilon_{Hf}(t)$ values (−8.28~2) and T_{DM2} = 2680–3141 Ma. These suggested that crustal remelting was the main form of crustal evolution in this period.

Above all, the remelting of old crust occurred almost all the time, and the Paleozoic and Neoproterozoic were the main crustal growth periods.

5.3.2. Tectonic Implication

(1) Tectonic implication from detrital zircon

Besides the crustal evolution reflected by the geochemical features of the detrital zircons, the message of tectonic events could also be read out and interpreted. The age of the zircons with strongly positive $\varepsilon_{Hf}(t)$ values was concentrated in 461~465 Ma, ~823 Ma, 982~1017 Ma, and 1426~1606 Ma. It indicated that in these periods, the zircons should be derived from a depleted mantle by magmatism very close to the extensional tectonic environment, while the age of the zircons with strongly negative $\varepsilon_{Hf}(t)$ values was concentrated in ~441 Ma, ~557 Ma, 760~782 Ma, and ~830 Ma. This group of zircons represented the melting of the ancient crust and its recycling, which may have happened in a collisional tectonic setting. Combined with the geological and historical story, the zircons aged 1426~1606 Ma with positive $\varepsilon_{Hf}(t)$ values should be close to the breakup of the Columbia supercontinent at ~1400 Ma. The Neoproterozoic zircons with strongly positive $\varepsilon_{Hf}(t)$ values should be close to the oceanic subduction during the formation of the Rodinia supercontinent at ~0.9~1.0 Ga, while the zircons with strongly negative $\varepsilon_{Hf}(t)$ values were almost marked by very old T_{DM2} (>2.5 Ga), suggesting they may have been derived from the crust during the formation of the Kenorland supercontinent.

(2) Tectonic setting in the Late Devonian

It has been shown that the chemical compositions of the sediments can be related to plate tectonic processes, making geochemistry a powerful tool for recognizing ancient tectonic settings [50,76–78]. The value of K_2O/Na_2O of sedimentary rock behaves differently from its SiO_2 content in different tectonic settings. Roser and Korsch [57] used K_2O/Na_2O-SiO_2 diagrams to distinguish the sedimentary rocks' tectonic settings successfully: active continental margin, passive continental margin, and island arc. The result shows that our samples are plotted in the fields of the active continental margin and island arc (Figure 12). Large ionic lithophile elements such as Th, Co, Zr, La, and Sc were also successfully used to distinguish the sedimentary rocks' tectonic environment. In the triangle series of diagrams proposed by Bahatia and Crook in 1986 [79], most of our samples are plotted in the continental arc (Figure 12) and active continental margin fields. There are also two samples plotted in the oceanic island arc field. It suggests that in the Late Devonian, the layers of the Xinghongpu Fm. were deposited in an active continental margin setting with arc systems. However, there was rare volcanism during the Devonian in the study area. The latest volcanic deposition occurred in the Late Silurian. Combined with the distributional characteristics of the zircon ages, the sedimentary rock in the Xinghongpu Fm. should contain a lot of re-depositional igneous clastic from Silurian.

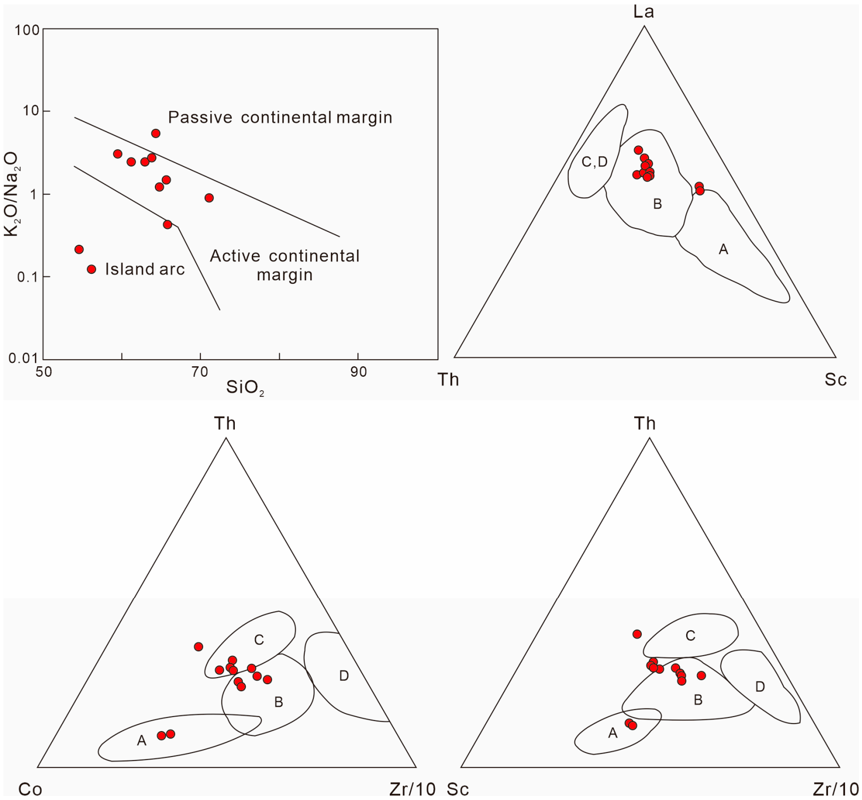

Figure 12. Tectonic discrimination diagrams for the Paleoproterozoic metasedimentary rocks (after Roser and Korsch, 1988 [57]; Bhatia and Crook, 1986 [79]). Abbreviations for tectonic settings: A, oceanic island arc; B, continental arc; C, active continental margin; D, passive continental margin.

6. Conclusions

The Xinghongpu Fm. was not deposited earlier than 363.2 Ma, which constrains its depositional age to the Late Devonian. The provenance of the Xinghongpu Fm. was mainly from quartzose sediments of mature continental provenance, while mafic and intermediate igneous provenances also contributed a bit. Ancient crusts from the NQB and the SQB were the main sources for the provenance of the metasedimentary layers in the Xinghongpu Fm. The tectonic setting of the Fengxian area in the central SQB is an oceanic basin in an active continental margin environment with arc systems in the Late Devonian. The regional crustal evolution was related to the breakup and formation of supercontinents such as Columbia and Rodinia. The age peak (700~950 Ma) of zircon showed a co-relationship with the formation (1.0~0.9 Ga) and breakup (750~720 Ma) of supercontinent Rodinia, showing recycling continental material marked with negative $\varepsilon_{Hf}(t)$ and the juvenile crust represented by the ones with the positive $\varepsilon_{Hf}(t)$. The zircons aged 2.1~1.7 Ga were all with negative $\varepsilon_{Hf}(t)$ values and may represent the formation of the supercontinent Columbia.

Supplementary Materials: The following supporting information can be downloaded at https://www.mdpi.com/article/10.3390/min13060768/s1: Table S1: Result of zircon U-Pb dating and Hf isotope; Table S2: Result of element geochemistry of samples.

Author Contributions: Conceptualization, Z.Z. and T.Z.; methodology, D.L.; software, T.Z. and H.W.; validation, Z.Z. and B.D.; formal analysis, D.Z.; investigation, Z.Z., B.D. and Y.Z.; resources, Z.Z.; data curation, B.D., C.Z. and Z.L.; writing—original draft preparation, Z.Z.; writing—review and editing, T.Z. and Y.S.; visualization, Z.Z., N.C. and X.Z.; supervision, Z.Z. and T.Z.; project administration, Z.Z., N.C. and X.Z.; funding acquisition, Z.Z. All authors have read and agreed to the published version of the manuscript.

Funding: This research was funded by the Shaanxi Youth Science and Technology Star Project (Grant No. 2021KJXX-87), the Shaanxi Public Welfare Geological Survey Project (Grant Nos. 20180301, 201918, 202103, and 202306), the Fundamental Research Funds for the Central Universities grant (Grant No. 18CX06019A), and the National Natural Science Foundation of China (41872235).

Data Availability Statement: The data presented in this study are available in supplementary material, which can be downloaded at: www.mdpi.com/xxx/s1.

Acknowledgments: The authors thank Kaijun Zhang and anonymous reviewers for their constructive suggestions and kind help during the modification process of this paper.

Conflicts of Interest: The authors declare no conflict of interest.

References

1. Zhang, G.W.; Meng, Q.R.; Lai, S.C. Tectonics and structure of the Qinling Orogenic belt. *Sci. Chin.* **1995**, *38*, 1379–1394.
2. Zhang, K.J. North and South China collision along the eastern and southern North China margins. *Tectonophysics* **1997**, *270*, 145–156. [CrossRef]
3. Meng, Q.R.; Zhang, G.W. Geologic framework and tectonic evolution of the Qinling orogen, central China. *Tectonophysics* **2000**, *323*, 183–196. [CrossRef]
4. Dong, Y.P.; Liu, X.M.; Santosh, M.; Chen, Q.; Zhang, X.N.; Li, W.; He, D.F.; Zhang, G.W. Neoproterozoic accretionary tectonics along the northwestern margin of the Yangtze Block, China: Constraints from zircon U–Pb geochronology and geochemistry. *Precambr. Res.* **2012**, *196–197*, 247–274. [CrossRef]
5. Dong, Y.P.; Liu, X.M.; Neubauer, F.; Zhang, G.W.; Tao, N.; Zhang, Y.G.; Zhang, X.N.; Li, W. Timing of Paleozoic amalgamation between the North China and South China Blocks: Evidence from detrital zircon U–Pb ages. *Tectonophysics* **2013**, *586*, 173–191. [CrossRef]
6. Tang, L.; Santosh, M.; Dong, Y.P. Tectonic evolution of a complex orogenic system: Evidence from the northern Qinling belt, central China. *J. Asian Earth Sci.* **2015**, *113*, 544–559. [CrossRef]
7. Santosh, M. Evolution of continents, cratons and supercontinents: Building the habitable Earth. *Curr. Sci.* **2013**, *104*, 871–879.
8. Santosh, M.; Yang, Q.Y.; Teng, X.M.; Tang, L. Paleoproterozoic crustal growth in the North China Craton: Evidence from the Lüliang Complex. *Precambrian Res.* **2015**, *263*, 197–231. [CrossRef]
9. Xiao, W.J.; Santosh, M. The western Central Asian Orogenic Belt: A window to accretionary orogenesis and continental growth. *Gondwana Res.* **2014**, *25*, 1429–1444. [CrossRef]
10. Zhang, G.W.; Meng, Q.R.; Yu, Z.P.; Sun, Y.; Zhou, D.W.; Guo, A.L. Orogenic process and dynamic characteristics of Qinling orogenic belt. *Sci. Chin. Ser. D* **1996**, *26*, 193–200, (In Chinese with English Abstract).
11. Zhang, K.J. Escape hypothesis for the North and South China collision and the tectonic evolution of the Qinling orogen, eastern Asia. *Eclogae Geol. Helv.* **2002**, *95*, 237–247.

12. Dong, Y.P.; Santosh, M. Tectonic architecture and multiple orogeny of the Qinling Orogenic Belt, Central China. *Gondwana Res.* **2016**, *29*, 1–40. [CrossRef]
13. Dong, Y.P.; Yang, Z.; Liu, X.M.; Zhang, X.N.; He, D.F.; Li, W.; Zhang, F.F.; Sun, S.S.; Zhang, H.F.; Zhang, G.W. Neoproterozoic amalgamation of the Northern Qinling terrain to the North China Craton: Constraints from geochronology and geochemistry of the Kuanping ophiolite. *Precambr. Res.* **2014**, *255*, 77–95. [CrossRef]
14. Tseng, C.Y.; Yang, H.J.; Yang, H.Y.; Liu, D.Y.; Wu, C.L.; Cheng, C.K.; Cheng, C.H.; Ker, C.M. Continuity of the North Qilian and North Qinling orogenic belts, Central Orogenic System of China: Evidence from newly discovered Paleozoic adakitic rocks. *Gondwana Res.* **2009**, *16*, 285–293. [CrossRef]
15. Shi, Y.; Yu, J.H.; Santosh, M.J.P.R. Tectonic evolution of the Qinling orogenic belt, Central China: New evidence from geochemical, zircon U–Pb geochronology and Hf isotopes. *Precambrian Res.* **2013**, *231*, 19–60. [CrossRef]
16. Diwu, C.; Sun, Y.; Zhao, Y.; Liu, B.X.; Lai, S.C. Geochronological, geochemical, and Nd-Hf isotopic studies of the Qinling Complex, central China: Implications for the evolutionary history of the North Qinling Orogenic Belt. *Geosci. Front.* **2014**, *5*, 499–513. [CrossRef]
17. Xue, F.; Kröner, A.; Reischmann, T.; Lerch, F. Palaeozoic pre-and post-collision calc-alkaline magmatism in the Qinling orogenic belt, central China, as documented by zircon ages on granitoid rocks. *J. Geol. Soc.* **1996**, *153*, 409–417. [CrossRef]
18. Wang, X.X.; Wang, T.; Haapala, I.; Mao, J. P–T conditions of crystallization and origin of plagioclase-mantled alkali feldspar megacrysts in the Mesozoic granitoids in the Qinling orogen (China). *Lithos* **2008**, *103*, 289–308. [CrossRef]
19. Weislogel, A.L.; Graham, S.A.; Chang, E.Z.; Wooden, J.L.; Gehrels, G.E.; Yang, H.S. Detrital zircon provenance of the late triassic songpan-ganzi complex: Sedimentary record of collision of the North and South China blocks. *Geology* **2006**, *34*, 97–100. [CrossRef]
20. Yu, J.H.; O'Reilly, S.Y.; Wang, L.; Griffin, W.L.; Zhang, M.; Wang, R.; Jiang, S.Y.; Shu, L. Where was South China in the Rodinia supercontinent?: Evidence from U–Pb geochronology and Hf isotopes of detrital zircons. *Precambrian Res.* **2008**, *164*, 1–15. [CrossRef]
21. Wu, F.Y.; Ji, W.Q.; Liu, C.Z.; Chung, S.L. Detrital zircon U–Pb and Hf isotopic data from the Xigaze fore-arc basin: Constraints on Transhimalayan magmatic evolution in southern Tibet. *Chem. Geol.* **2010**, *271*, 13–25. [CrossRef]
22. Cawood, P.A.; Hawkesworth, C.; Dhuime, B. Detrital zircon record and tectonic setting. *Geology* **2012**, *40*, 875–878. [CrossRef]
23. Zhang, Y.X.; Zeng, L.; Li, Z.W.; Wang, C.S.; Zhang, K.J.; Yang, W.G.; Gao, T.L. Late Permian–Triassic siliciclastic provenance, palaeogeography, and crustal growth of the Songpan terrane, eastern Tibetan Plateau: Evidence from U–Pb ages, trace elements, and Hf isotopes of detrital zircons. *Int. Geol. Rev.* **2015**, *57*, 159–181. [CrossRef]
24. Yang, W.T.; Yang, J.H.; Wang, X.F.; Du, Y.S. Uplift-denudation history of the qinling orogen: Constrained from the detrital-zircon U–Pb geochronology. *J. Asian Earth Sci.* **2014**, *89*, 54–65. [CrossRef]
25. Zhang, Y.X.; Zeng, L.; Zhang, K.J.; Li, Z.W.; Wang, C.S.; Guo, T.L. Late Paleozoic and Early Mesozoic tectonic and paleogeographic evolution of central China: Evidence from U–Pb and Lu–Hf isotope systematics of detrital zircons from the western Qinling region. *Int. Geol. Rev.* **2014**, *56*, 351–392. [CrossRef]
26. Li, K.; Guo, A.L.; Gao, C.Y.; Li, X.H. A tentative discussion on the source area of the Late Triassic Liuyehe basin in North Qinling Mountains and its relationship with the Ordos basin: Evidence from LA-ICP-MS U-Pb dating of detrital zircons. *Geol. Bull. China* **2015**, *34*, 1426–1437.
27. Gao, C.Y.; Guo, A.L.; Li, X.H.; Li, K.; Liu, W.G. LA-ICP-MS U-Pb dating of detrital zircon from Liuyehe basin in North Qinling Mountains. *Geol. Bull. China* **2015**, *34*, 1689–1698.
28. Li, X.H.; Guo, A.L.; Li, K.; Gao, C.Y. LA-ICP-MS U-Pb dating of detrital zircon from Lingguanmiao basin in North Qinling. *Geol. Bull. China* **2014**, *33*, 1353–1362.
29. Wang, Z.Y.; Pei, X.Z.; Li, R.B.; Pei, L.; Li, Z.C.; Liu, C.J.; Zhao, S.W.; Wang, M.; Chen, Y.X.; Zhou, H.; et al. Middle Neoproterozoic Tectonic Evolution of the Mianlue Tectonic Belt: Evidences from Detrital Zircon U-Pb Geochronology and Geochemistry of the Guantianmen Metasedimentary Rocks in Lueyang County. *Geoscience* **2022**, *36*, 770–795. [CrossRef]
30. Dai, Y.Q.; Luo, J.L.; Wang, M.; Li, M.; Bai, X.J.; Yan, L.W.; Cheng, C. Geochemical characteristics and provenance of meta-mudsiltstones from the Danfeng ophiolite mélange in eastern Qinling, central China. *Geol. Bull. China* **2009**, *28*, 1465–1471.
31. Chen, Y.L.; Li, D.P.; Zhou, J.; Zhang, H.F.; Liu, F.; Nie, L.S.; Jiang, L.T.; Liu, X.M. U-Pb ages of zircons in Western Qinling Mountain, China and their tectonic implications. *Earth Sci. Front.* **2008**, *15*, 088–107. [CrossRef]
32. Chen, L.Y.; Luo, Y.L.; Liu, X.C.; Qu, W.; Hu, J. LA-ICP-MS U-Pb geochronology of detrital zircons from the Liuling Group in the South Qinling tectonic belt and its tectonic significance. *Geol. Bull. China* **2014**, *33*, 1363–1378. (In Chinese with English Abstract).
33. Li, Y.F.; Yang, C.M.; Fan, J.; Zhao, M. Geological Significance of Detrital Zircon U-Pb Age of Middle Devonian Proximal Sedimentary Rocks in Boyang Town, Western Qinling Orogenic Belt. *Northwestern Geol.* **2017**, *50*, 92–104. (In Chinese with English Abstract).
34. Li, Y.F.; Luo, J.H.; Xu, H.; You, J.; Chen, G.X. Detrital Zircon U-Pb Age, Geochemical Characteristics and Geological Significance of Meta-sandstones form Boyang—Yuanlong Area in The Western Qinling Orogenic Belt. *Geol. Rev.* **2018**, *64*, 1087–1102. (In Chinese with English Abstract).
35. Mao, C. Genesis of Gold and Lead-Zinc Deposits in Fengxian Area, South Qinling. Ph.D. Thesis, China University of Geosciences, Beijing, China, 2019.
36. Yang, N.; Zhang, Z.K.; Yang, J.H.; Hong, Z.L.; Shi, J. A convolutional neural network of GoogLeNet applied in mineral prospectivity prediction based on multi-source geoinformation. *Nat. Resour. Res.* **2021**, *30*, 3905–3923. [CrossRef]

37. Chen, Y.J.; Chen, H.Y.; Zaw, K.; Pirajno, F.; Zhang, Z.J. Geodynamic settings and tectonic model of skarn gold deposits in China: An overview. *Ore Geol. Rev.* **2007**, *31*, 139–169. [CrossRef]
38. Mao, S.D.; Chen, Y.J.; Zhou, Z.J.; Lu, Y.H. U-Pb ages of detrital zircon grains from the donghe group in the southern qinling microcontinent: Implications for tectonic evolution. *Acta Petrol. Sin.* **2013**, *29*, 67–82.
39. Kimura, T. Relationships between inorganic elements and minerals in coals from the Ashibetsu district, Ishikari coal field, Japan. *Fuel Process Technol.* **1998**, *56*, 1–19. [CrossRef]
40. Liang, Q.; Jing, H.; Gregoire, D.C. Determination of trace elements in granites by inductively coupled plasma mass spectrometry. *Talanta* **2000**, *51*, 507–513. [CrossRef]
41. Wiedenbeck, M.A.P.C.; Alle, P.; Corfu, F.Y.; Griffin, W.L.; Meier, M.; Oberli, F.V.; Spiegel, W. Three natural zircon standards for U-Th-Pb, Lu-Hf, trace element and REE analyses. *Geostand. Newsl.* **1995**, *19*, 1–23. [CrossRef]
42. Ludwig, K.R. User's manual for Isoplot 3.00: A geochronological toolkit for Microsoft Excel (No. 4). *Berkeley Geochronl. Cent. Spec. Publ.* **2003**, *4*, 25–32.
43. Duan, L. Detrital Zircon Provenance of the Silurian and Devonian in South Qingling, and the Northwestern Margin of Yangtze Terrane and Its Tectonic Implications. Master's Thesis, P.R.C. Northwest University, Xi'an, China, 2010.
44. Meng, E.; Wang, C.Y.; Li, Y.G.; Li, Z.; Yang, H.; Cai, J.; Ji, L.; Jin, M.Q. Zircon U–Pb–Hf isotopic and whole-rock geochemical studies of Paleoproterozoic metasedimentary rocks in the northern segment of the Jiao–Liao–Ji Belt, China: Implications for provenance and regional tectonic evolution. *Precambrian Res.* **2017**, *298*, 472–489. [CrossRef]
45. Chu, N.C.; Taylor, R.N.; Chavagnac, V.; Nesbitt, R.W.; Boella, R.M.; Milton, J.A.; German, C.R.; Bayon, G.; Burton, K. Hf isotope ratio analysis using multicollector inductively coupled plasma mass spectrometry: An evaluation of isobaric interference corrections. *J. Anal. At. Spectrom.* **2002**, *17*, 1567–1574. [CrossRef]
46. Scherer, E.; Münker, C.; Mezger, K. Calibration of the lutetium-hafnium clock. *Science* **2001**, *293*, 683–687. [CrossRef]
47. Griffin, W.L.; Pearson, N.J.; Belousonva, E.; Jackson, S.E.; van Achterbergh, E.; O'Reilly, S.Y.; Shee, S.R. The Hf isotope composition of cratonic mantle: LA-MCICP-MS analysis of zircon megacrysts in kimberlites. *Geochim. Cosmochim. Acta* **2000**, *64*, 133–147. [CrossRef]
48. Griffin, W.L.; Belousova, E.A.; Shee, S.R.; Pearson, N.J.; O'Reilly, S.Y. Archean crustal evolution in the northern Yilgam Craton: U-Pb and Hf-isotope evidence from detrital zircons. *Precambr. Res.* **2004**, *131*, 231–282. [CrossRef]
49. Herron, M.M. Geochemical classification of terrigenous sands and shales from core or log data. *J. Sediment. Petrol.* **1988**, *58*, 820–829.
50. Taylor, S.R.; Mclennan, S.M. The Continental Crust: Its Composition and Evolution. In *An Examination of the Geochemical Record Preserved in Sedimentary Rocks*; Blackwell Scientific Pub: Hoboken, NJ, USA, 1985; pp. 1–311.
51. Zhou, T.F.; Zhou, Y.Q.; Zhao, H.J.; Li, M.J.; Mu, H.Y. Depositional Setting and Enrichment Mechanism of Organic Matter of Lower Cretaceous Shale in Ri-Qing-Wei Basin in the Central Sulu Orogenic Belt. *Front. Earth Sci.* **2022**, *9*, 808916. [CrossRef]
52. Hoskin, P.W.; Ireland, T.R. Rare earth element chemistry of zircon and its use as a provenance indicator. *Geology* **2000**, *28*, 627–630. [CrossRef]
53. Belousova, E.A.; Griffin, W.L.; O'Reilly, S.Y.; Fisher, N.L. Igneous zircon: Trace element composition as an indicator of source rock type. *Contrib. Mineral. Petrol.* **2002**, *143*, 602–622. [CrossRef]
54. Tomaschek, F.; Kennedy, A.K.; Villa, I.M.; Lagos, M.; Ballhaus, C. Zircons from Syros, Cyclades, Greece-recrystallization and mobilization of zircon during high-pressure metamorphism. *J. Petrol.* **2003**, *44*, 1977–2002. [CrossRef]
55. Dubińska, E.; Bylina, P.; Kozłowski, A.; Dörr, W.; Nejbert, K.; Schastok, J.; Kulicki, C. U–Pb dating of serpentinization: Hydrothermal zircon from a metasomatic rodingite shell (Sudetic ophiolite, SW Poland). *Chem. Geol.* **2004**, *203*, 183–203. [CrossRef]
56. Yang, P.; Huang, Q.T.; Zhang, K.J.; Argyrios, K.; Zheng, H.; Peng, T.P.; Zhou, R.J.; Yang, Q.K.; Luo, W.X.; Xia, B. Compositional signatures of ophiolitic rocks from the Dongco massif: Novel insights into the evolution of the central Tibetan Meso-Tethyan oceanic plateau. *Lithos* **2022**, *416–417*, 106660. [CrossRef]
57. Roser, B.P.; Korsch, R.J. Provenance signatures of sandstone-mudstone suites determined using discriminant function analysis of major-element data. *Chem. Geol.* **1988**, *67*, 119–139. [CrossRef]
58. Floyd, P.A.; Leveridge, B.E. Tectonic environment of the devonian gramscatho basin, south cornwall: Framework mode and geochemical evidence from turbiditic sandstones. *J. Geol. Soc.* **1987**, *144*, 531–542. [CrossRef]
59. McLennan, S.M.; Hemming, S.; McDaniel, D.K.; Hanson, G.N. Geochemical approaches to sedimentation, provenance, and tectonics. *Spec. Pap. Geol. Soc. Am.* **1993**, *21*, 129996010.
60. Condie, K.C.; Noll, P.D., Jr.; Conway, C.M. Geochemical and detrital mode evidence for two sources of Early Proterozoic sedimentary rocks from the Tonto Basin Supergroup, central Arizona. *Sediment. Geol.* **1992**, *77*, 51–76. [CrossRef]
61. Qin, Z.W.; Wu, Y.B.; Siebel, W.; Gao, S.; Wang, H.; Abdallsamed, M.I.; Zhang, W.X.; Yang, S.H. Genesis of adakitic granitoids by partial melting of thickened lower crust and its implications for early crustal growth: A case study from the Huichizi pluton, Qinling orogen, central China. *Lithos* **2015**, *238*, 1–12. [CrossRef]
62. Liu, C.H.; Wu, C.L.; Gao, Y.H.; Lei, M.; Qin, H.P.; Li, M.Z. Zircon LA-ICP-MS U-Pb dating and Lu-Hf isotopicsystem of Dongjiangkou, Zhashui, and Liyuantang granitoid intrusions, South Qinling belt, central China. *Acta Petrol. Sin.* **2014**, *30*, 2402–2420. (In Chinese with English Abstract).

63. Zhu, X.Y.; Chen, F.; Li, S.Q.; Yang, Y.Z.; Nie, H.; Siebel, W.; Zhai, M.G. Crustal evolution of the North Qinling terrain of the Qinling Orogen, China: Evidence from detrital zircon U–Pb ages and Hf isotopic composition. *Gondwana Res.* **2011**, *20*, 194–204. [CrossRef]
64. Olierook, H.K.; Barham, M.; Fitzsimons, I.C.; Timms, N.E.; Jiang, Q.; Evans, N.J.; McDonald, B.J. Tectonic controls on sediment provenance evolution in rift basins: Detrital zircon U–Pb and Hf isotope analysis from the Perth Basin, Western Australia. *Gondwana Res.* **2019**, *66*, 126–142. [CrossRef]
65. Gehrels, G. Detrital Zircon U-Pb Geochronology Applied to Tectonics. *Annu. Rev. Earth Planet. Sci.* **2014**, *42*, 127–149. [CrossRef]
66. Hu, J.; Liu, X.C.; Chen, L.Y.; Qu, W.; Li, H.K.; Gen, J.Z. A ~2.5 Ga magmatic event at the northern margin of the Yangtze craton: Evidence from U-Pb dating and Hf isotope analysis of zircons from the Douling Complex in the South Qinling orogen. *Chin. Sci. Bull.* **2013**, *58*, 3564–3579. [CrossRef]
67. Jiang, Y.H.; Liao, S.Y.; Yang, W.Z.; Shen, W.Z. An island arc origin of plagiogranites at Oytag, western Kunlun orogen, northwest China: SHRIMP zircon U–Pb chronology, elemental and Sr–Nd–Hf isotopic geochemistry and Paleozoic tectonic implications. *Lithos* **2008**, *106*, 323–335. [CrossRef]
68. Zhao, T.F.; Lin, B.L.; Chen, C.X.; Wang, C.; Li, L. Petrogenisis and geological significance of Neoproterozoic gneissic biotite monzogranite in Akechukesai area, western segment of the east Kunlun Orogenic belt, Qinghai province: Constraints from geochemistry, zircon U-Pb chronology and Hf isotopes. *J. Jilin Univ.* **2022**, *52*, 1540–1557. (In Chinese with English Abstract). [CrossRef]
69. Chen, N.S.; Gong, S.L.; Sun, M.; Li, X.Y.; Xia, X.P.; Wang, Q.Y.; Wu, F.Y.; Xu, P. Precambrian evolution of the Quanji Block, northeastern margin of Tibet: Insights from zircon U–Pb and Lu–Hf isotope compositions. *J. Asian Earth Sci.* **2009**, *35*, 367–376. [CrossRef]
70. Zheng, J.P.; Griffin, W.L.; O'Reilly, S.Y.; Lu, F.X.; Yu, C.M.; Zhang, M.; Li, H.M. U–Pb and Hf-isotope analysis of zircons in mafic xenoliths from Fuxian kimberlites: Evolution of the lower crust beneath the North China Craton. *Contrib. Mineral. Petrol.* **2004**, *148*, 79–103. [CrossRef]
71. Yang, J.H.; Wu, F.Y.; Liu, X.M.; Xie, L.W. Zircon U-Pb ages and Hf isotopes and their geological significance of the Miyun rapakivi granites from Beijing, China. *Acta Petrol. Sin.* **2005**, *21*, 1633–1644. (In Chinese with English Abstract).
72. Peng, M.; Wu, Y.B.; Gao, S.; Zhang, H.F.; Wang, J.; Liu, X.C.; Gong, H.J.; Zhou, L.; Hu, Z.C.; Liu, Y.S.; et al. Geochemistry, zircon U–Pb age and Hf isotope compositions of Paleoproterozoic aluminous A-type granites from the Kongling terrain, Yangtze Block: Constraints on petrogenesis and geologic implications. *Gondwana Res.* **2012**, *22*, 140–151. [CrossRef]
73. Xu, X.S.; Griffin, W.L.; Ma, X.; O'Reilly, S.Y.; He, Z.Y.; Zhang, C.L. The Taihua group on the southern margin of the North China craton: Further insights from U–Pb ages and Hf isotope compositions of zircons. *Mineral. Petrol.* **2009**, *97*, 43–59. [CrossRef]
74. Zhao, J.H.; Zhou, M.F.; Zheng, J.P.; Fang, S.M. Neoproterozoic crustal growth and reworking of the Northwestern Yangtze Block: Constraints from the Xixiang dioritic intrusion, South China. *Lithos* **2010**, *120*, 439–452. [CrossRef]
75. Zhao, J.H.; Zhou, M.F. Neoproterozoic adakitic plutons in the northern margin of the Yangtze Block, China: Partial melting of a thickened lower crust and implications for secular crustal evolution. *Lithos* **2008**, *104*, 231–248. [CrossRef]
76. Bhatia, M. Plate tectonics and geochemical composition of sandstones. *J. Geol.* **1983**, *91*, 611–627. [CrossRef]
77. Zhang, Z.K.; Zhou, Y.Q.; Zhou, T.F.; Yu, S.S.; He, Y.F.; Gao, F. Geochemistry of siltstones of the Early Cretaceous Laiyang Group in Taolin area, Shandong Province, Eastern China: Implications for provenance, source weathering, palaeoenvironment, and tectonic setting. *Geol. J.* **2018**, *55*, 133–146. [CrossRef]
78. Zhou, T.F.; Zhou, Y.Q.; Søager, N.; Holm, P.M.; Zhang, Z.K.; Wang, J.; Liang, Z.; Mu, H.Y.; Cheng, Y.J.; Liu, F.F.; et al. Late Mesozoic rifting and its deep dynamic mechanisms in the central Sulu orogenic belt: Records from Lingshan Island. *Sci. China Earth Sci.* **2022**, *65*, 1751–1771. [CrossRef]
79. Bhatia, M.R.; Crook, K.A. Trace element characteristics of graywackes and tectonic setting discrimination of sedimentary basins. *Contrib. Mineral. Petrol.* **1986**, *92*, 181–193. [CrossRef]